Research Square

Preprints are preliminary reports that have not undergone peer review.
They should not be considered conclusive, used to inform clinical practice,
or referenced by the media as validated information.

Bayesian seismic fragility curves for building components based on questionnaire damage data from the 2016 Kumamoto and 2022 Fukushima-ken Oki earthquakes

Takahiro Matsui

t_matsui@shimz.co.jp

Institute of Technology, Shimizu Corporation

Takeshi Morii

Institute of Technology, Shimizu Corporation

Rie Okazawa

Institute of Technology, Shimizu Corporation

Tomoaki Nishino

Kyoto University

Hiroaki Notake

Institute of Technology, Shimizu Corporation

Aya Hada

Kyoto University

Research Article

Keywords: Fragility curve, Nonstructural building component, Equipment, Questionnaire survey, Nonlinear seismic response analysis, Bayesian inference

Posted Date: November 16th, 2026

DOI: https://doi.org/10.21203/rs.3.rs-11550932/v1

License: This work is licensed under a Creative Commons Attribution 4.0 International License.
Read Full License

Additional Declarations: No competing interests reported.

Bayesian seismic fragility curves for building components based on questionnaire damage data from the 2016 Kumamoto and 2022 Fukushima-ken Oki earthquakes

Takahiro Matsui [1]*, Takeshi Morii [1], Rie Okazawa [1], Tomoaki Nishino [2], Hiroaki Notake [1], and Aya Hada [2]

[1] Institute of Technology, Shimizu Corporation, 3-4-17 Etchujima, Koto-ku, Tokyo 135-8530, Japan

[2] Disaster Prevention Research Institute, Kyoto University, Gokasho, Uji, Kyoto 611-0011, Japan

*Corresponding author. E-mail: t_matsui@shimz.co.jp, ORCID: https://orcid.org/0009-0006-0484-1415

Acknowledgements

This study was supported by the Academia-Industry Collaborative Research Program involving Kyoto University, Tokyo Polytechnic University, Shimizu Corporation, and the Ohsaki Research Institute, Japan. The authors are grateful to the respondents from the surveyed buildings who completed the questionnaire. The authors also acknowledge the use of observed ground motions from the National Research Institute for Earth Science and Disaster Resilience (K-NET and KiK-net), the Japan Meteorological Agency, and local governments. The authors thank Editage for English language editing.

Abstract

Assessments of the damage states of building components caused by earthquakes are a critical element in estimating economic and functional losses. The Federal Emergency Management Agency (FEMA) has developed fragility curves for various types of building components as a function of structural response quantities. However, the applicability of these fragility curves to Japanese buildings remains uncertain because building design standards and construction practices vary substantially between countries and regions. This study developed empirical fragility curves based on damage data from past earthquakes in Japan using a Bayesian approach, allowing the characteristics of existing fragility curves in FEMA P-58 to be incorporated into the inference as prior information. The data were collected through questionnaire surveys of 24 buildings affected by the 2016 Kumamoto and 2022 Fukushima-ken Oki earthquakes. The observed damage states of 13 types of building components (columns and beams, exterior walls, partition walls, window panes, ceilings, interior doors, lighting fixtures, sinks and toilets, air conditioners, fire doors, fire sprinkler heads, plumbing, and elevators) were correlated with the structural response quantities estimated through nonlinear seismic response analyses using multi-degree-of-freedom shear building models. The resulting 18 Bayesian fragility curves (including different damage states) showed dependence on whether informative or weakly informative prior distributions were used, suggesting that not only the new survey dataset but also the existing fragility curves were reflected in the developed fragility curves. This demonstrates that these curves can serve as tools for achieving more reasonable seismic damage assessments of building components for potential future earthquakes in Japan.

Keywords Fragility curve, Nonstructural building component, Equipment, Questionnaire survey, Nonlinear seismic response analysis, Bayesian inference

1. Introduction

Assessments of the damage states of building components caused by earthquakes are a critical element in estimating economic and functional losses. In particular, recent earthquake damage surveys have shown that even when structural components remain intact, damage to nonstructural components and equipment has led to significant economic losses, casualties, and functional failures (Filiatrault and Sullivan 2014; Perrone et al. 2019; Achour and Miyajima 2020). Furthermore, there have been cases in which the restoration of these components required considerable time (Filiatrault and Sullivan 2014; Achour and Miyajima 2020; Nishino 2024). Consequently, within the framework of Performance-Based Earthquake Engineering (Günay and Mosalam 2013; Heresi and Miranda 2023), it is now necessary to evaluate damage to individual building components. Given that nonstructural components and equipment account for more than 50% of total construction costs (Taghavi and Miranda 2003; Casagrande et al. 2019), evaluating their damage is a high priority. Damage states are generally assessed using fragility curves, which model the relationship between the probability of exceeding specific damage levels and seismic intensities or structural response quantities. While numerous fragility curves for overall building damage exist (Rossi et al. 2020; Donà et al. 2021; Zuccaro et al. 2021; Ioannou et al. 2025), the development of fragility curves for building components and their specific damage states remains limited, making the development of such curves increasingly important.

Fragility curves are developed using post-earthquake damage assessment data, experimental data, numerical analyses, or expert opinions (Porter et al. 2007). For instance, fragility curves have been proposed for structural components, nonstructural components, and equipment using damage datasets from the 2000 and 2008 earthquakes in Iceland (Moosapoor et al. 2025) and for structural and nonstructural components of RC buildings using data from damage survey conducted after the 2015 Nepal earthquake (Gautam et al. 2021). However, these curves use peak ground acceleration (PGA) as an intensity measure because the target buildings are low-rise structures. Consequently, these studies (Moosapoor et al. 2025; Gautam et al. 2021) do not incorporate structural response quantities as intensity measures, limiting their applicability at the building level and across construction types and precluding the quantitative evaluation of seismic retrofitting effectiveness. Fragility curves based on structural response quantities have been developed using damage data from the 1995 Hyogo-ken Nanbu earthquake (Suwa and Kanda 2008). However, these structural response quantities are estimated using regression equations as functions of peak ground velocity (PGV), and notable data dispersion is observed around the regression equations, resulting in low estimation accuracy. Furthermore, fragility

curves in these studies (Suwa and Kanda 2008; Moosapoor et al. 2025) grouped nonstructural components and equipment with similar installation patterns and uses, making it impossible to evaluate damage states specific to each component. To date, few studies have developed fragility curves for building components and their various damage states using actual damage data on building components caused by earthquakes, apart from fragility curves for fire doors based on damage data from the 1995 Hyogo-ken Nanbu earthquake (Nishino et al. 2025), likely owing to the rarity of detailed damage data. The Federal Emergency Management Agency (FEMA) has organized the relationship between damage states of building components and structural response quantities, such as peak interstory drift angle (PIDA) and peak floor acceleration (PFA), based on experimental data and has developed fragility curves for structural and nonstructural components and equipment (FEMA 2018a, b, c). Structural and nonstructural components and equipment are classified according to factors such as material, dimensions, and construction methods used in the U.S., and fragility curves are developed for each damage level. The applicability of these curves to Japanese buildings remains uncertain because building design standards and construction practices vary significantly between countries and regions. Nevertheless, fragility curves in FEMA P-58 can be considered valuable information for developing fragility curves for building components, as they clearly organize the relationships between structural response quantities and damage states across various structural and nonstructural components and equipment. Developing fragility curves for building components in each country requires data on structural response quantities and building component damage that reflect local design standards and construction methods. However, collecting a large amount of such data is difficult. To address these limitations, applying Bayesian inference is an effective approach. Bayesian inference is a method that enables accurate posterior estimation even when the sample size is small by incorporating reliable existing knowledge as prior distributions. For example, Wang et al. (2018) developed fragility curves by estimating their parameters through Bayesian inference using actual earthquake damage data on nuclear power plant equipment, with simulation results obtained using the finite element method serving to construct the prior distributions. This approach incorporated actual damage observations that could not be fully captured by simulation alone, thereby improving estimation accuracy.

Accordingly, this study developed fragility curves based on Bayesian inference, combining prior distributions derived from fragility curves in FEMA P-58 with actual damage data from Japan. Specifically, questionnaire surveys were conducted following two earthquake events that caused damage to buildings to collect as much data as possible on damage to building components. Furthermore, the damage states of building components were correlated with the

estimated structural response quantities derived from nonlinear seismic response analysis. The novelty of this study lies in two aspects. First, fragility curves were developed using actual damage data from building components affected by earthquakes in Japan and estimated structural response quantities derived from nonlinear seismic response analysis, enabling damage assessment of individual building components based on empirically validated structural response quantities. Second, Bayesian inference was employed to leverage prior information from experimental fragility curves in FEMA P-58 and effectively integrate observational data, thereby improving estimation accuracy.

The remainder of this paper is organized as follows. Section 2 describes the methods for developing fragility curves. It presents an overview of the questionnaire survey results from the 2016 Kumamoto and 2022 Fukushima-ken Oki earthquakes. Datasets for fragility curves are developed by relating damage states from the surveys to the estimated structural response quantities derived from nonlinear seismic response analysis. Formulas for the fragility curves are defined, and explanatory variables characterizing the damage states of each building component and the uncertainties considered are detailed. Prior distributions based on FEMA P-58 are created, and a method for estimating fragility curves using Bayesian inference and survey data is outlined. Section 3 presents the 18 fragility curves for 13 types of building components, developed using the methods described in Section 2, and discusses their applicability. It also examines the effects of prior distribution types and data quantity on estimation accuracy. The discussion includes differences in damage states among building components and relationships between them. It also addresses the issues encountered in this study. Finally, Section 4 concludes the study.

2. Methods

Fig. 1 illustrates the technical flow of this study for developing empirical seismic fragility curves for building components. The study employed a three-step method: (1) collecting earthquake damage data through questionnaire surveys, (2) estimating structural response quantities for the surveyed buildings through nonlinear seismic response analyses, and (3) correlating the observed damage with the estimated structural response quantities through Bayesian regression analyses using informative priors, yielding empirical seismic fragility curves. Damage to 24 key building component types, including structural and architectural nonstructural components and electrical, sanitary, HVAC, vertical transport, and life safety equipment, was surveyed with a particular focus on two recent large earthquakes in

Japan. These earthquakes were the 2016 Kumamoto earthquake, which struck Kumamoto, southwestern Japan, on April 16, 2016 (1:25 a.m. local time) with a moment magnitude of 7.3 (NIED 2019a), and the 2022 Fukushima-ken Oki earthquake, which struck off the coast of Fukushima, northeastern Japan, on March 16, 2022 (11:36 p.m. local time) with a moment magnitude of 7.4 (NIED 2019a). The selection of these earthquakes was based on the following considerations. (1) The 2022 Fukushima-ken Oki earthquake was the most recent large earthquake in Japan as of the survey (in 2023) to affect regional cities; this earthquake did not cause severe damage to structural components, while it is likely that nonstructural components suffered slight to severe damage. (2) The 2016 Kumamoto earthquake was one of the most destructive inland earthquakes in Japan to affect regional cities; it is likely that this earthquake caused slight to severe damage to both structural and nonstructural components, unlike the 2022 Fukushima-ken Oki earthquake. In the nonlinear seismic response analyses, multi-degree-of-freedom (MDOF) shear building models that characterize the actual yield strength of Japanese buildings were employed given the difficulty of obtaining structural drawings. Meanwhile, the analyses were limited to buildings located in the vicinity of seismic stations to allow the use of observed ground motion waveforms given the inherent limitations of ground motion simulations. PIDA and PFA were estimated for each floor given that the surveyed building components included both deformation-sensitive and acceleration-sensitive components. Following the typical procedure for developing fragility curves, the cumulative distribution function of a lognormal distribution was fitted to the data. Notably, Bayesian inference was employed to incorporate knowledge from existing experimental fragility curves in FEMA P-58 into the regression as informative priors, resulting in 18 Japan-specific fragility curves based on actual earthquake damage, encompassing 13 building component types and different damage states.

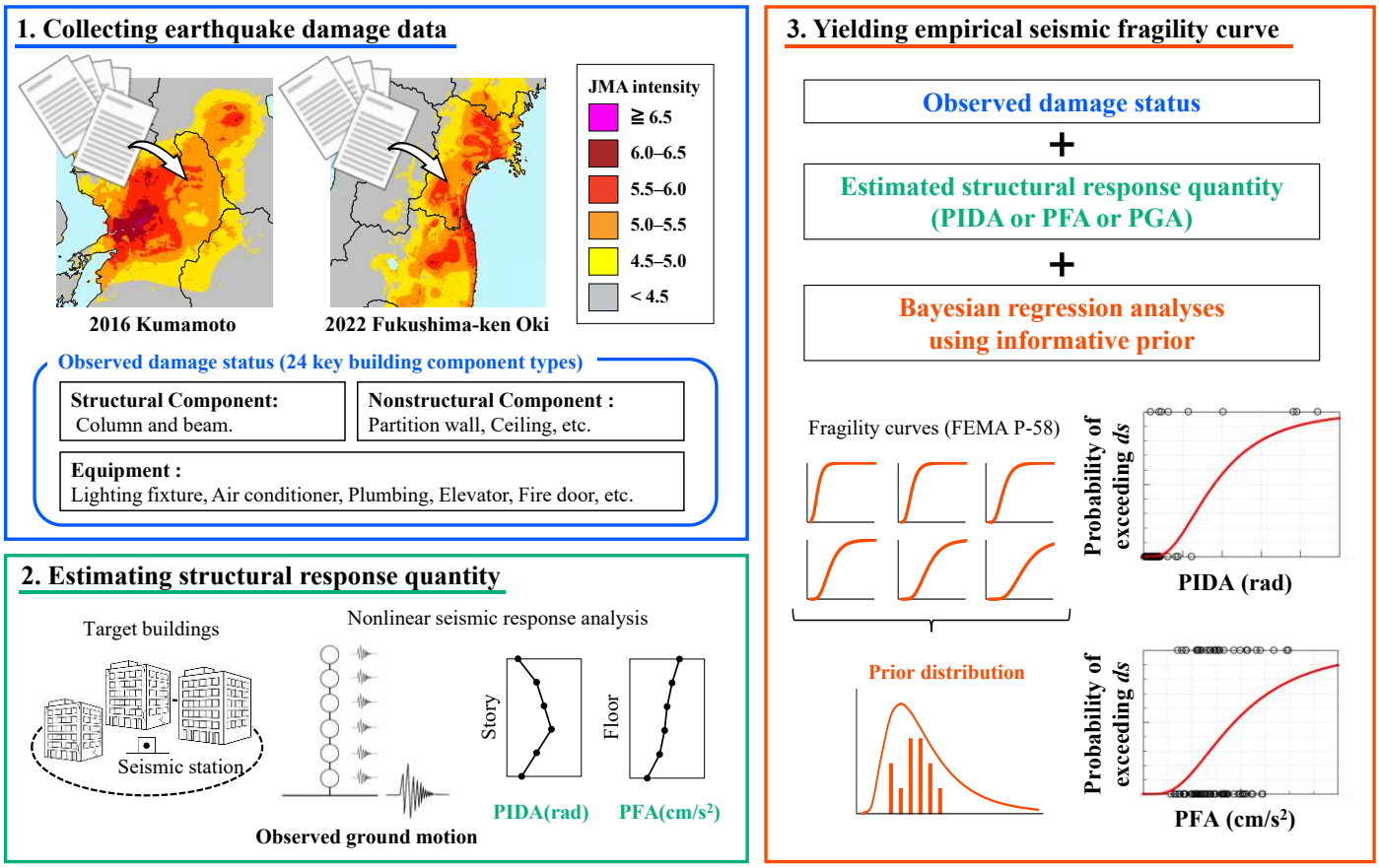


Fig. 1 Technical flow diagram for developing empirical seismic fragility curves for building components based on actual earthquake-induced damage data.

2.1 Data collection

Self-administered questionnaires were mailed to 1,272 buildings that were estimated to have experienced Japan Meteorological Agency (JMA) instrumental seismic intensities of 5.0 or greater during the 2016 Kumamoto and 2022 Fukushima-ken Oki earthquakes. These buildings were selected from a broad range of buildings beyond areas near seismic stations in order not only to develop fragility curves but also to investigate recovery times and business continuity status. These buildings comprise four use types, namely, local government offices, hospitals, hotels, and nursing homes. These use types were selected for the following reasons: (1) they are expected to provide reliable responses owing to well-established management practices; and (2) contact information for questionnaire distribution was readily available. The target buildings were determined using the estimated JMA instrumental seismic intensity maps (Fig. 2) provided by QuiQuake (National Institute of Advanced Industrial Science and Technology (AIST) 2013), which is a system capable of producing maps displaying estimated ground motion intensities based on records observed by nationwide strong-motion seismograph networks operated by the National Research Institute for Earth Science and

Disaster Resilience of Japan. The JMA intensity criterion (i.e., an intensity of 5.0) corresponds to ground motions that cause difficulty in walking and initiate cracking in the structural frames of reinforced concrete buildings with low seismic performance (Japan Meteorological Agency 2009). For the 2016 Kumamoto earthquake, the questionnaires were mailed on September 13, 2024, to 36 local government offices, 169 hospitals, 72 hotels, and 116 nursing homes; consequently, 60 completed questionnaires were collected before November 1, 2024, including those from 12 local government offices, 26 hospitals, 6 hotels, and 16 nursing homes. For the 2022 Fukushima-ken Oki earthquake, the questionnaires were mailed on September 1, 2023, to 124 local government offices, 228 hospitals, 182 hotels, and 345 nursing homes; consequently, 182 completed questionnaires were collected before October 13, 2023, including those from 50 local government offices, 39 hospitals, 20 hotels, and 73 nursing homes. The response rates were approximately 15% for the 2016 Kumamoto earthquake and 21% for the 2022 Fukushima-ken Oki earthquake. The considerable time that had elapsed since the 2016 Kumamoto earthquake may have contributed to the relatively low response rate compared with that for the 2022 Fukushima-ken Oki earthquake.

Damage to 24 key building component types was surveyed. Specifically, the components surveyed were (1) columns and beams, (2) exterior walls, (3) partition walls, (4) window panes, (5) interior doors, (6) ceilings, (7) power receiving and transforming equipment, (8) electrical wiring, (9) lighting fixtures, (10) emergency generators, (11) water reservoir tanks, (12) water tanks on the rooftop, (13) water supply pumps, (14) boilers, (15) plumbing, (16) sinks and toilets, (17) bathtubs, (18) air conditioners, (19) condenser units, (20) air ducts, (21) elevators, (22) fire doors, (23) fire detectors, and (24) fire sprinkler heads. These components were classified into two types based on their installation characteristics: (1) floor-specific components typically installed on each floor (e.g., partition walls and ceilings) and (2) building-wide components installed at a single location or spanning multiple floors (e.g., water reservoir tanks and elevators). For the former, the questionnaires asked for the specific floors where damage occurred, while for the latter, damage was surveyed at the building level. As shown in Fig. 3, the questionnaires for partition walls, which are components installed on each floor, were designed to allow respondents to provide information concerning which floors the damage was observed using a multiple-choice format. Several states representing slight to severe damage were defined for each component and were specified in the questionnaires to allow respondents to objectively evaluate damage. As an example, two damage states, namely, cracking and falling, were specified for partition walls. The specified damage states for all the components are listed in Table 1. For columns and beams,

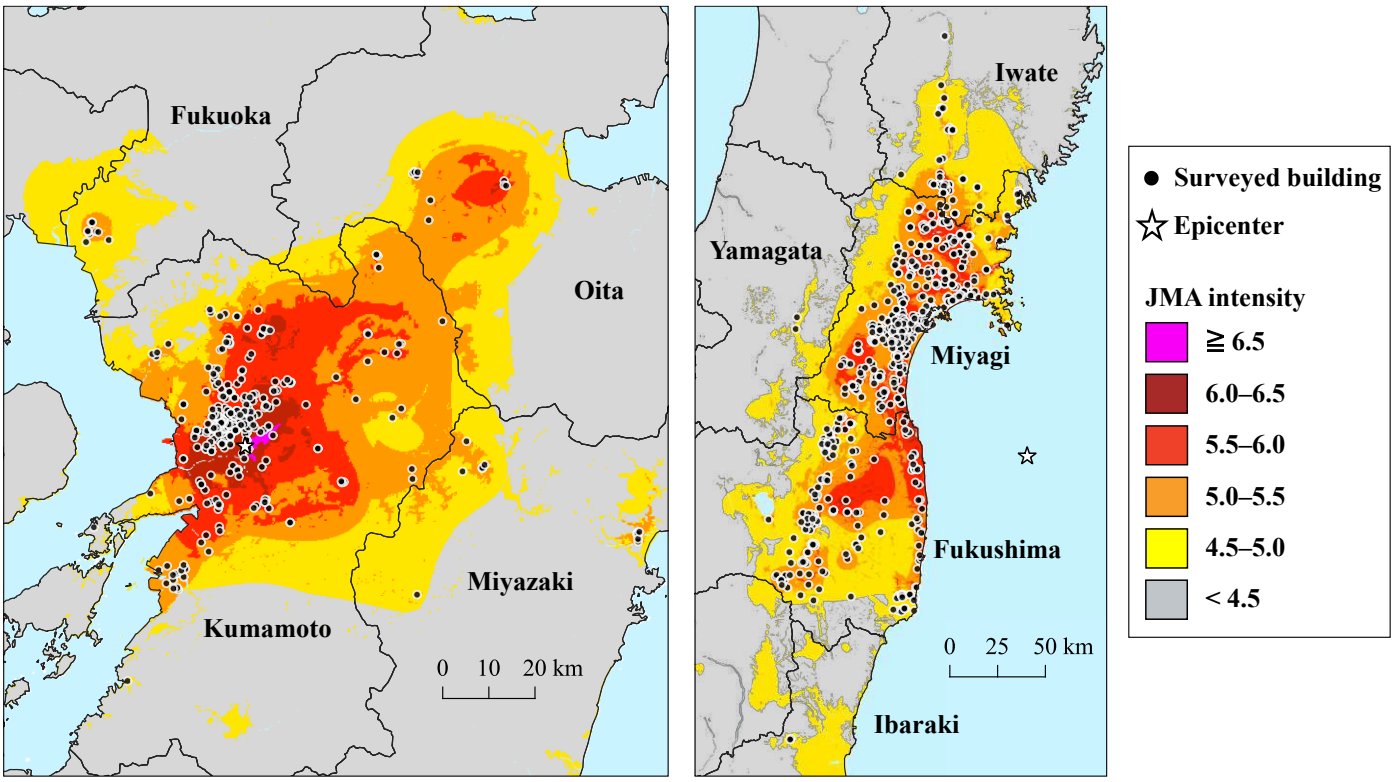
exterior walls, partition walls, and ceilings in particular, photographs illustrating the specified damage states were included in the questionnaires with supplementary explanations to allow respondents to visually recognize them and minimize misunderstandings. Additionally, the following key building attributes were surveyed: (1) the construction type, (2) the construction year, (3) the number of floors, (4) the total floor area, (5) the footprint area, (6) the presence or absence of seismic retrofitting, (7) the presence or absence of a base-isolation system, (8) the building damage grade assessed by local governments, and (9) the presence or absence of demolition or rebuilding after the earthquake. The respondents were defined as individuals knowledgeable about building component damage caused by the earthquakes and the subsequent restoration, including facility or disaster management staff. In instances where multiple buildings were located at a single address, responses were obtained for one representative building or the most heavily damaged building. Note that the questionnaires included questions regarding the time to restoration of each component; however, the details and analyses of these responses are omitted from this study because they will be addressed in a separate study (Nishino et al. 2026).

Buildings that met the following criteria were selected for analysis to effectively use observed ground motion waveforms: (1) they were located within 500 m of their nearest seismic stations; (2) their site amplification factors (NIED 2019b), specifically the amplification of PGV from engineering bedrock, where Vs = 400 m/s, to the ground surface, did not significantly differ from those at their nearest seismic stations, specifically with a difference of less than 0.05; and (3) they were regular buildings that conformed to the modeling conditions of the analytical model described below. Irregular buildings with large differences in floor area between stories were excluded. Regularity was assessed based on the number of stories, total floor area, and footprint area reported in the questionnaire survey. Consequently, the buildings analyzed—the majority of which were local government offices—consisted of 5 buildings affected by the 2016 Kumamoto earthquake and 19 buildings affected by the 2022 Fukushima-ken Oki earthquake, excluding buildings with base-isolation systems. This analysis yielded a pair of observed damage and estimated structural response quantities for each floor of the 24 buildings, resulting in a dataset of 90 floors. Damage patterns and structural response levels vary by floor, even within the same building, with each floor providing a distinct pair of observed damage and estimated response quantities. The floor-level damage dataset includes 90 samples, which is sufficient for the statistical analyses conducted in this study. In contrast, the building-level damage dataset includes 24 samples and is relatively small; however, because the sample size exceeds 20, it is still considered acceptable for statistical analysis. The analyzed

buildings were reinforced concrete (RC) or steel-framed reinforced concrete (SRC) buildings, comprising 18 with 2–4 stories and 6 with 5–7 stories. The number of buildings constructed before and after the revision of the Japanese building code in 1981 were 10 and 14, respectively. Among the buildings constructed before 1981, five underwent seismic retrofitting. It should be noted that, for two buildings affected by the 2016 Kumamoto earthquake, detailed damage was reported through on-site investigations (Fujii 2019; Mukai et al. 2021), and the data were corrected accordingly.

Fig. 4 shows damage ratios for structural components, nonstructural components, and equipment from the questionnaire survey conducted following the 2016 Kumamoto and 2022 Fukushima-ken Oki earthquakes. Fig. 4a shows the damage ratios relative to the total number of buildings, and Fig. 4b shows the damage ratios relative to the total number of stories. Unanswered questions were considered invalid. Damage rates relative to the total number of buildings showed that the rates of water leakage from plumbing and emergency stops of elevators for safety inspections exceeded 20%, indicating high rates. By contrast, damage rates for rooftop water tanks, deformation/cracking in plumbing, air duct damage, and transport equipment were approximately 5–10%, with the number of buildings reporting damage ranging from one to three. No buildings reported damage to power-receiving and transforming equipment, emergency generators, water reservoir tanks, or water supply pumps. In terms of damage rates relative to the total number of stories, relatively minor damage such as cracking in columns, beams, exterior walls, and partition walls, displacement/cracking in ceilings, and interior clutter accounted for over 20% of cases. Severe damage, including rebar exposure in columns and beams, falling partition walls, and falling ceilings, was low at around 5–10%. Damage to electrical wiring and fire detectors was extremely low (less than 5%), with no buildings reporting damage to bathtubs.

Given these damage ratios, 13 building component types with a certain number of instances of damage were selected for fragility curve development. Including different damage states, 18 fragility curves were developed in total. These curves were for (1) cracking in columns and beams, (2) peeling of columns and beams, (3) rebar exposure in columns and beams, (4) cracking of exterior walls, (5) peeling of exterior walls, (6) cracking in partition walls, (7) falling partition walls, (8) damage to window panes, (9) damage to interior doors, (10) displacement/cracking in ceilings, (11) falling ceilings, (12) displacement/cracking in lighting fixtures, (13) damage to sinks and toilets, (14) damage to air conditioners, (15) damage to fire doors, (16) damage to fire sprinkler heads, (17) water leakage from plumbing, and (18) emergency stops of elevators for safety inspections.



(a) 2016 Kumamoto (b) 2022 Fukushima-ken Oki

Fig. 2 Estimated Japan Meteorological Agency (JMA) instrumental seismic intensity maps for (a) the 2016 Kumamoto earthquake and (b) the 2022 Fukushima-ken Oki earthquake, with epicenters indicated by stars and buildings to which questionnaires were mailed indicated by black circles.

(2-3) Partition wall

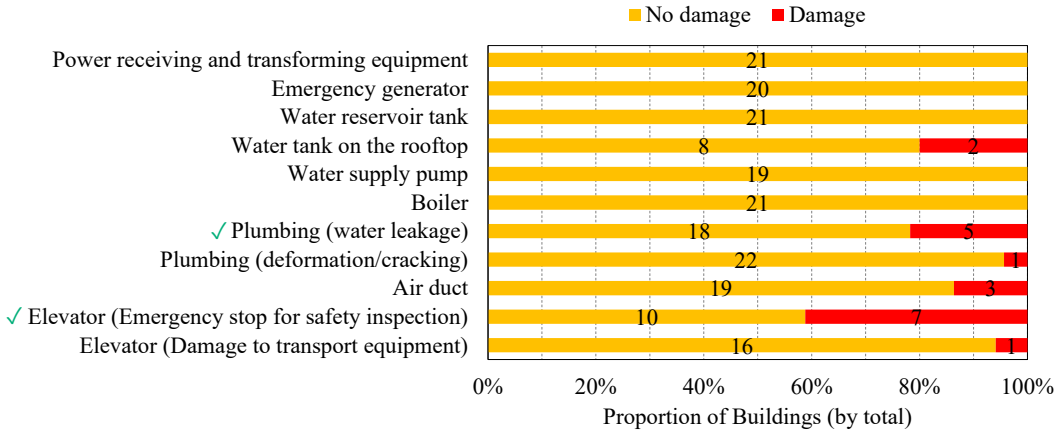
Floors where damage was observed (multiple answers allowed)	**Cracking** ☐ None ☐ 1st floor ☐ 2nd floor ☐ 3rd floor ☐ 4th floor ☐ 5th floor ☐ 6th floor ☐ 7th floor ☐ 8th floor ☐ 9th floor ☐ 10th floor or higher
	Falling ☐ None ☐ 1st floor ☐ 2nd floor ☐ 3rd floor ☐ 4th floor ☐ 5th floor ☐ 6th floor ☐ 7th floor ☐ 8th floor ☐ 9th floor ☐ 10th floor or higher

Fig. 3 Questionnaire sample with questions concerning partition wall damage.

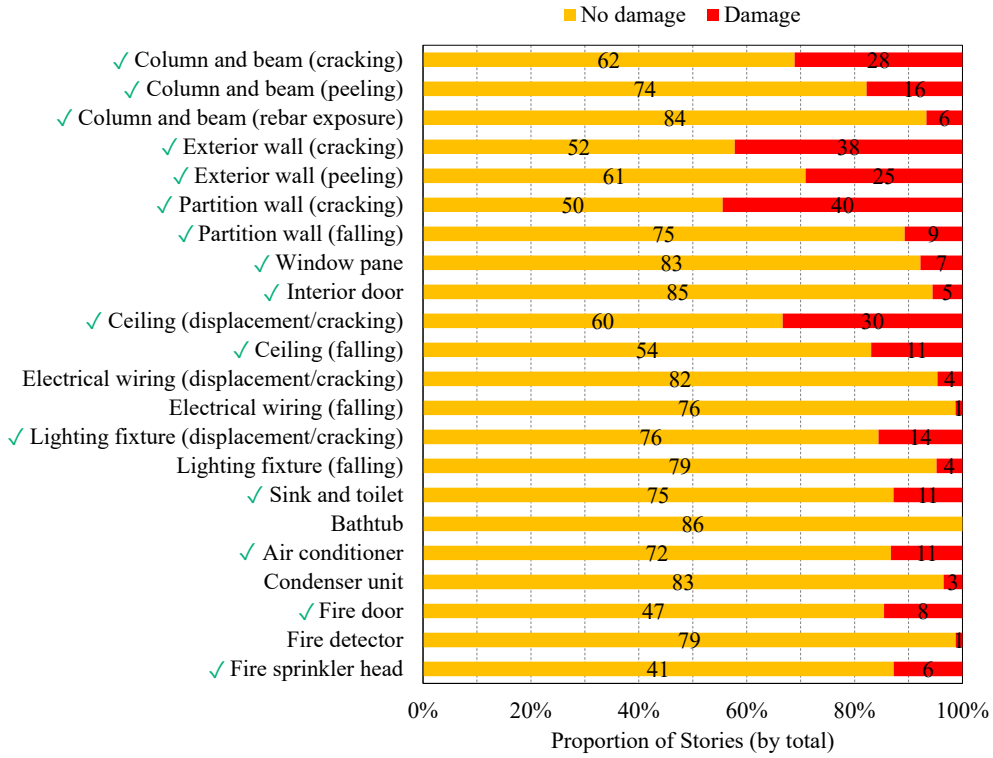
Table 1 Definitions of damage states for structural and nonstructural components provided in the questionnaire.

Category	Building component	Damage state	Installation type
Structural component	Column and beam	Cracking, peeling, rebar exposure	Story
Nonstructural	Exterior wall	Cracking, peeling	Story

component	Partition wall	Cracking, falling	Story
	Window pane	Overall damage	Story
	Interior door	Overall damage	Story
	Ceiling	Displacement/cracking, falling	Story
Equipment	Power receiving and transforming equipment	Mounting part failure, damage to equipment	Building
	Electrical wiring	Displacement/cracking, falling	Story
	Lighting fixture	Displacement/cracking, falling	Story
	Emergency generator	Mounting part failure, damage to equipment	Building
	Water reservoir tank	Mounting part failure, damage to the tank, damage to pipe connection, water leakage	Building
	Water tank on the rooftop	Mounting part failure, damage to the tank, damage to pipe connection, water leakage	Building
	Water supply pump	Mounting part failure, damage to the pump, damage to pipe connection, water leakage	Building
	Boiler	Mounting part failure, damage to the boiler	Building
	Plumbing	Water leakage, deformation/cracking	Building
	Sink and toilet	Overall damage	Story
	Bathtub	Overall damage	Story
	Air conditioner	Overall damage	Story
	Condenser unit	Overall damage	Story
	Air duct	Overall damage	Building
	Elevator	Emergency stop for safety inspection, damage to transport equipment	Building
	Fire door	Overall damage	Story
	Fire detector	Overall damage	Story
	Fire sprinkler head	Overall damage	Story



(a) Numbers on bar chart correspond to number of buildings with and without damage.



(b) Numbers on bar chart correspond to number of stories with and without damage.

Fig. 4 Damage status of buildings in the 2016 Kumamoto and 2022 Fukushima-ken Oki earthquakes. Items without parentheses represent overall damage, and checkmarks indicate building components for which fragility curves were developed.

2.2 Building model

MDOF shear building models were developed individually for each analyzed building using building attribute information from the questionnaire surveys, including the construction type, the construction year, the number of floors, and the footprint area. As described in Section 2.1, the analyzed buildings were non-isolated RC or SRC buildings with

two or more stories constructed before or after the revision of the Japanese building code in 1981. However, the effect of different construction types was neglected; that is, SRC buildings were modeled as RC buildings. This treatment was adopted for the following reasons: (1) fundamental natural periods and base shear coefficients are typically similar between RC and SRC buildings (Okazawa et al. 2018); and (2) the seismic response of SRC buildings is sometimes analyzed using the same trilinear restoring force characteristics as RC buildings (Nakamura et al. 2013; Morita and Kashima 2017; Okazawa et al. 2018).

As shown in Fig. 5, the building models are multi-mass models with nonlinear shear springs between two adjacent floors. The floor-to-floor height and floor mass of a given building model are assumed to be uniform across all floors. The springs are assumed to have hysteretic restoring force characteristics based on the modified Takeda model (Takeda et al. 1970), as shown in Fig. 6. The base shear coefficient C_B was determined using the average strength distribution for RC structures proposed by Nagato and Kawase (2004), based on the number of floors and construction year, as listed in Table 2. This C_B was calculated to reproduce the damage rate observed during the 1995 Hyogo-ken Nanbu earthquake. Setting this C_B accounts for the fact that the actual strength of RC buildings exceeds the design value, thereby reducing errors in the estimated structural response quantities from the analysis model. For seismically retrofitted buildings, the base shear coefficient from 1982 onward was used. The vertical distribution of seismic load was determined using the Ai distribution (Aoyama 1981; Umemura et al. 1984). Assuming a story height of 3.5 m, the building height H_i [m] of the i^{th} building was $H_i = 3.5n_i$, where n_i is the number of floors. The mass m_{ij} [kg] of the j^{th} floor of the i^{th} building was calculated by multiplying the footprint area by the mass per unit area of 1.0 t/m^2 and was assumed to be uniform across all floors. The fundamental natural period T_i [s] was set as $T_i = 0.02H_i$. The initial stiffness $K_{1,ij}$ [N/mm] was calculated by assuming a linear distribution of stiffness between the first floor and the top floor of the building at a ratio of 2:1, and then back-calculated to match T_i. The yield strength $Q_{y,ij}$ [N] was calculated as $Q_{y,ij} = C_{B,i}\, Ai_{ij} \sum_{k=j}^{n_i} m_{ik}\, g$, where g is the gravitational acceleration [m/s^2]. The first inflection point of the restoring force characteristic was set to one-third of the yield capacity $Q_{y,ij}$, and the yield deformation angle R_y [rad] was set to 1/150 rad for all stories. The second stiffness $K_{2,ij}$ [N/mm] was determined from the first inflection point and the yield deformation angle R_y. The third stiffness $K_{3,ij}$ [N/mm] was set to 0.01 times $K_{1,ij}$. The damping ratio was set to 3% for instantaneous stiffness-proportional damping.

The input ground motions for nonlinear seismic response analysis were acceleration waveforms obtained from

seismic stations near the buildings (K-NET, KiK-net (NIED 2019c), JMA stations, and local government stations). Observed ground motions were input in two horizontal directions (NS and EW), and the direction with the largest PIDA was adopted. Fig. 7 shows the relationship between PGA and PGV of the ground motions used as input for nonlinear seismic response analysis. The PGV was less than 50 cm/s for the 2022 Fukushima-ken Oki earthquake, but three records exceeded 50 cm/s for the 2016 Kumamoto earthquake. The predominant periods T_{eq} calculated as $T_{eq} = 2\pi \cdot \mathrm{PGV/PGA}$, where PGV is in cm/s and PGA is in cm/s², were mostly in the 0.3–1.0 s range. These values are longer than the fundamental natural periods of 2–4-story buildings (0.14–0.28 s), which constitute a large portion of the target buildings. Fig. 8 shows the relationship between PIDA and PFA obtained from the nonlinear seismic response analysis of the buildings. The response values for two buildings with reported damage during the 2016 Kumamoto earthquake (Fujii 2019; Mukai et al. 2021) are also included after modification. However, since only PIDA was provided for one of these buildings (Mukai et al. 2021), the figure presents results for 85 stories across 23 buildings, excluding that one. The PIDA of this excluded building was large, ranging from approximately 0.01 to 0.04 rad. The PIDA ranged from 0.0003 to 0.022 rad, whereas the PFA ranged from 284 to 1490 cm/s². The PIDA exceeded the yield deformation angle R_y = 1/150 rad for only three older buildings subjected to the 2016 Kumamoto earthquake ground motions with PGV values exceeding 50 cm/s. For the 2022 Fukushima-ken Oki earthquake, which accounts for over half of the data, the PIDA values were below R_y, consistent with the survey results showing a low percentage of rebar exposure in columns and beams.

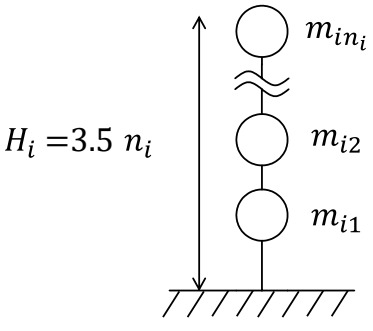


Fig. 5 MDOF shear building model (the i^{th} building).

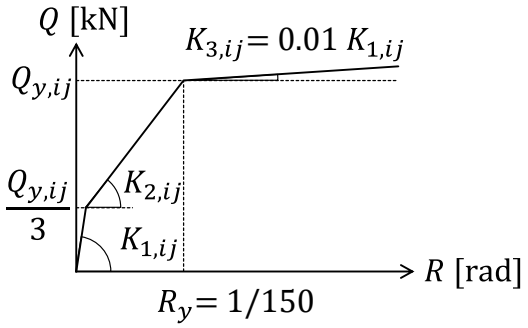


Fig. 6 Hysteretic restoring force characteristics (the i^{th} building, j^{th} story).

Table 2 Mean base shear coefficients by number of floors and construction year of buildings (Nagato and Kawase 2004).

Building construction year	Number of floors in buildings			
	2–4	5–7	8–10	11–13
Before or in 1981	0.96	0.70	0.30	0.41
In or after 1982	1.41	1.09	0.58	0.30

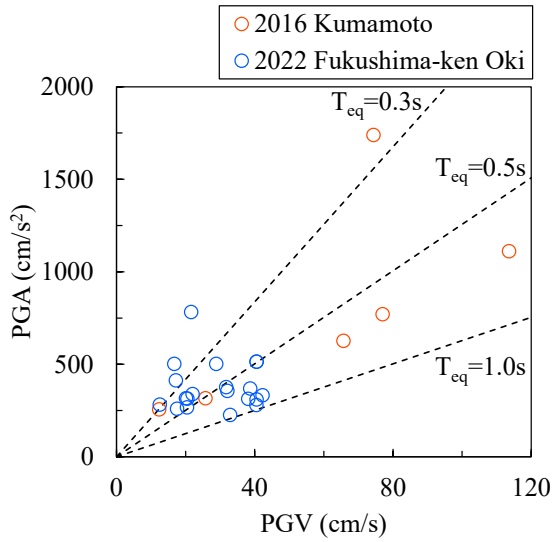


Fig. 7 PGA and PGV of observed ground motions used as input for nonlinear seismic response analysis.

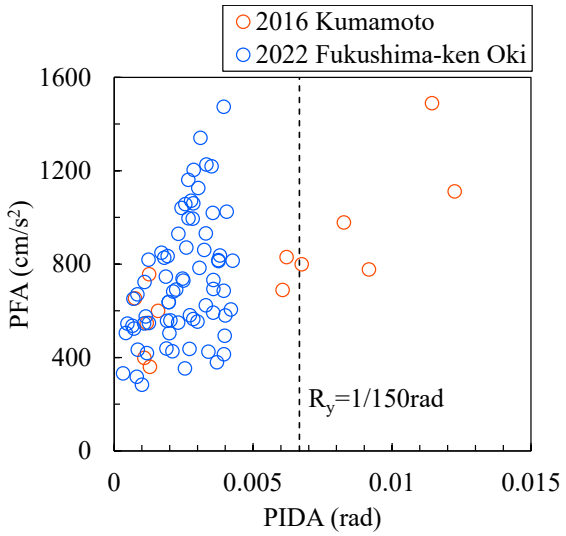


Fig. 8 PIDA and PFA of 85 stories calculated from nonlinear seismic response analysis.

2.3 Fragility curves

Following typical fragility function fitting procedures (Porter et al. 2007; Suwa and Kanda 2008; Cremen and Baker 2019; Gautam et al. 2021; Moosapoor et al. 2025), the observed building component damage on each story of the 24 considered buildings was linked to the calculated PIDA, PFA, or PGA, often called engineering demand parameter (edp), using the cumulative distribution function of a lognormal distribution. Let edp_{ij} be the calculated PIDA or PFA for the j^{th} floor of the i^{th} building, or PGA. The probability that the damage state of the building component on the j^{th} floor of the i^{th} building, DS_{ij}, exceeds the damage level, ds, is given by

$$f\left(DS_{ij} \geq ds \middle| edp_{ij}\right) = \Phi\left[\frac{ln\left(edp_{ij}/\theta\right)}{\beta}\right] \tag{1}$$

where Φ is the cumulative distribution function of the standard normal distribution, θ is the median, and β is the logarithmic standard deviation.

For deformation-sensitive component types, including columns and beams, exterior walls, partition walls, window panes, interior doors, fire doors, and plumbing, PIDA was used. However, for water leakage from plumbing, which causes damage to the entire building, the maximum PIDA value across all floors was used. For acceleration-sensitive component types, including ceilings, lighting fixtures, sinks and toilets, air conditioners, and fire sprinkler heads, PFA was used. For ceilings, lighting fixtures, air conditioners, and sprinkler heads, PFA at one floor above the installation floor was used. For emergency stops of elevators for safety inspections, an S-wave detector was assumed to have been installed at the bottom of the elevator shaft, and PGA was used.

When constructing fragility curves based on the relationship between the damage reported in the questionnaires and the estimated structural response quantities, uncertainties include (1) estimation errors in the structural response quantities; (2) variations in floor area across buildings and floors; and (3) variations in the specifications and construction quality of building components within each building. To address uncertainty (1), estimation errors in structural response quantities were minimized by restricting the analysis to buildings located within 500 m of seismic observation stations where the surface ground amplification ratio did not vary, using the recorded ground motions as input, and incorporating the actual lateral strengths of buildings estimated in previous studies rather than their design strengths into the analytical models. To address uncertainty (2), the analysis was restricted to regularly shaped buildings in which the floor area did not differ significantly across floors, thereby reducing the uncertainty arising from floor-to-floor variations in area. However, variations in floor area among buildings were unavoidable and remained a source of uncertainty. It should be noted that a larger floor area is associated with increased susceptibility to damage, as more building components are exposed to seismic loads. The fragility curves in FEMA P-58 primarily account for uncertainty (3), setting β to approximately 0.2 to 0.6 (FEMA 2018a, b, c). Specifically, for equipment fragility curves, when there is considerable uncertainty regarding equipment installation conditions, design methods, or fixation states, β is set to 0.6 (Eidinger 2009). Therefore, this study minimized uncertainty (1) as much as possible, while considering uncertainties (2) and (3), and set β to a relatively large value of 0.6.

2.4 Bayesian inference

The medians of the fragility curves were estimated using a Bayesian approach to incorporate knowledge from experimental fragility curves in FEMA P-58 (FEMA 2018a, b, c) as prior information. As mentioned earlier, many of the fragility curves in FEMA P-58 were developed from the results of shake table and static loading tests. Although the construction and associated uncertainties of these curves vary, they can be considered prior information for θ because these curves define the relationship between the structural response quantity and the probability of damage.

Fragility curves for each building component relative to the estimated structural response quantities were determined by setting β = 0.6, as described in Section 2.3, and performing Bayesian inference of θ based on the prior distribution. Bayesian inference is also possible by setting a prior distribution for β. However, determining an optimal value for β, which is an indicator of variability, from small samples of empirical data is not particularly meaningful. Rather, β

should be set based on uncertainties inherent in the fragility curves determined in this study. Let D denote a dataset comprising pairs of damage occurrences and the estimated structural response quantities. Then, the posterior distribution of θ, $p(\theta|D)$, is proportional to the product of the likelihood, $L(D|\theta)$, and the prior distribution, $p(\theta)$, according to Bayes' theorem:

$$p(\theta|D) = \frac{L(D|\theta)p(\theta)}{p(D)} \propto L(D|\theta)p(\theta) \tag{2}$$

where the likelihood $L(D|\theta)$ can be expressed as shown in Equation (3) for N buildings, based on the presence or absence of damage, r_{ij} (a binary value of 1 or 0), on the j^{th} floor of the i^{th} building and the structural response quantity edp_{ij}.

$$L(D|\theta) = \prod_{i=1}^{N}\prod_{j=1}^{n_i}\left\{\Phi\left[\frac{ln\,(edp_{ij}/\theta)}{\beta}\right]\right\}^{r_{ij}}\left\{1-\Phi\left[\frac{ln\,(edp_{ij}/\theta)}{\beta}\right]\right\}^{1-r_{ij}} \tag{3}$$

A prior distribution $p(\theta)$ can be set in two ways, depending on the availability of prior information: (1) an informative prior distribution and (2) a weakly informative prior distribution. Prior distributions for the fragility-curve medians were derived from fragility curves in FEMA P-58. If the damage states of the building components from the questionnaire surveys corresponded to two or more fragility curves in FEMA P-58, the lognormal distribution (Fig. 9a) given in Equation (4) was established as an informative prior distribution.

$$p(\theta) \sim Lognormal(\mu,\sigma) = \frac{1}{\sqrt{2\pi}\sigma\theta}exp\left\{-\frac{1}{2}\left(\frac{ln\,\theta-\mu}{\sigma}\right)^2\right\} \quad (\theta > 0) \tag{4}$$

where μ andσ are the median and standard deviation of $ln\,\theta$. μ and σ are calculated using the maximum median value θ'_{max} and minimum median value θ'_{min} of the FEMA P-58 fragility curves for each building component as follows:

$$\mu = \frac{ln\,\theta'_{max} + ln\,\theta'_{min}}{2} \tag{5}$$

$$\sigma = \frac{ln\,\theta'_{max} - ln\,\theta'_{min}}{2} \tag{6}$$

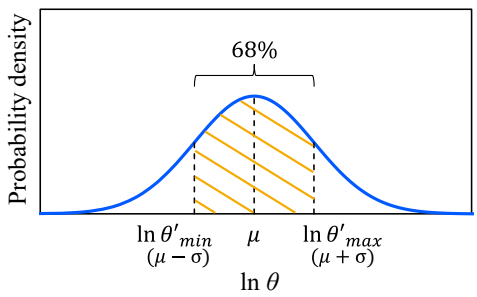
The lognormal distribution set by Equations (5) and (6) is defined such that the interval from $ln\,\theta'_{min}$ to $ln\,\theta'_{max}$ corresponds to $\mu \pm \sigma$ (approximately 68%) applies. However, when corresponding fragility curves are unavailable in FEMA P-58, a uniform distribution over the interval from a to b as shown in Equation (7), is set as a weakly informative prior distribution (Fig. 9b).

$$p(\theta) \sim Uniform\,(a, b) = \frac{1}{b-a} \tag{7}$$

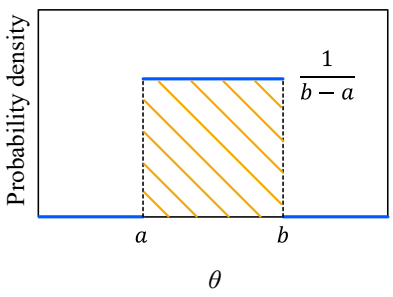
The posterior distributions of θ were obtained using Hamiltonian Monte Carlo sampling (Neal 2011) in Stan (Stan Development Team 2026). Four Markov chains with different initial values were used to generate samples from the distribution proportional to the product of the likelihood and prior distribution of θ. Samples deemed to have converged to the equilibrium distribution were used to characterize the posterior distribution of θ. For each chain, 6,000 samples were generated. The first 3,000 samples, presumed to depend on the initial values, were discarded, and the remaining 3,000 were retained. Thus, a total of 12,000 samples were used to determine the posterior distribution of θ. For convergence diagnostics, the Gelman–Rubin statistic $\hat{R}$ (Gelman and Rubin 1992) was used. When the value of $\hat{R}$ is 1.1 or less, the posterior distribution of θ is considered to have converged.

Among the 13 building component types selected in Fig. 4, the informative prior distributions were set for five types: columns and beams, exterior walls, partition walls, window panes, and ceilings. The parameters of the informative prior distributions are listed in Table 3, and the informative prior distributions are shown in Fig. 10. Table 3 presents the FEMA P-58 fragility curves used to establish the prior distribution for each building component. For columns and beams, exterior walls, partition walls, window panes, and ceilings, the general specifications of standard components were used as prior information. Therefore, seismically retrofitted building components were not used as reference information for the prior distribution. This exclusion was made because the survey results indicated that many buildings had not undergone seismic retrofitting of equipment or similar components. In FEMA P-58, the fragility curves are defined based on member dimensions and similar factors, even for building components with the same specifications. These variations were incorporated into the prior information. Regarding the damage states defined in FEMA P-58, the damage state most closely corresponding to each state defined in the questionnaire surveys was selected. The procedure for setting the informative prior distributions for partition walls and ceilings is described below as an example. In FEMA P-58, the damage states for gypsum board partition walls are defined as follows: DS1 (screw pop-outs and cracking of wallboards), DS2 (moderate cracking or crushing of gypsum wallboards and corner gap openings), and DS3 (buckling of studs, large gap openings, and displacement of walls). The parameters of the FEMA P-58 fragility curves differ depending on stud material, partition height, and top joint method. In the questionnaire surveys, two damage states were defined for partition walls: “cracking” and “falling”. Based on the similarity of the damage states, “cracking” was mapped to DS1 and DS2 in FEMA P-58, while “falling” was mapped to DS3 in FEMA P-58 to establish the informative

prior distributions. For ceilings, damage states in FEMA P-58 are defined based on the percentage of damaged ceiling area and do not distinguish between damage states such as displacement/cracking and falling. The parameters of the FEMA P-58 fragility curves differ depending on the types of standard ceiling areas. For the "displacement/cracking" and "falling" ceiling damage states defined in the questionnaire surveys, DS1 through DS3 in FEMA P-58 were used to establish the informative prior distributions. For lighting fixtures, air conditioners, plumbing, and elevators, fragility curves are defined in FEMA P-58; however, an informative prior distribution could not be established owing to the small number of fragility curves and differences in the assumed ds and edp. Additionally, FEMA P-58 provides no reference for other building components. Thus, Bayesian inference with a weakly informative prior distribution was applied to nonstructural components and equipment, excluding the aforementioned five types (columns and beams, exterior walls, partition walls, window panes, and ceilings). For components highly correlated with PIDA, a uniform distribution over the range from 0 to 0.1 rad was assigned as the weakly informative prior distribution. For components correlated with PFA or PGA, a uniform distribution over the range from 0 to 3,000 cm/s² was established as the weakly informative prior distribution, and the median value of the fragility curve was estimated using Bayesian inference. These upper limits were set to sufficiently cover the expected maximum structural responses of the analyzed buildings.



(a) Informative prior distribution: Lognormal (μ,σ).



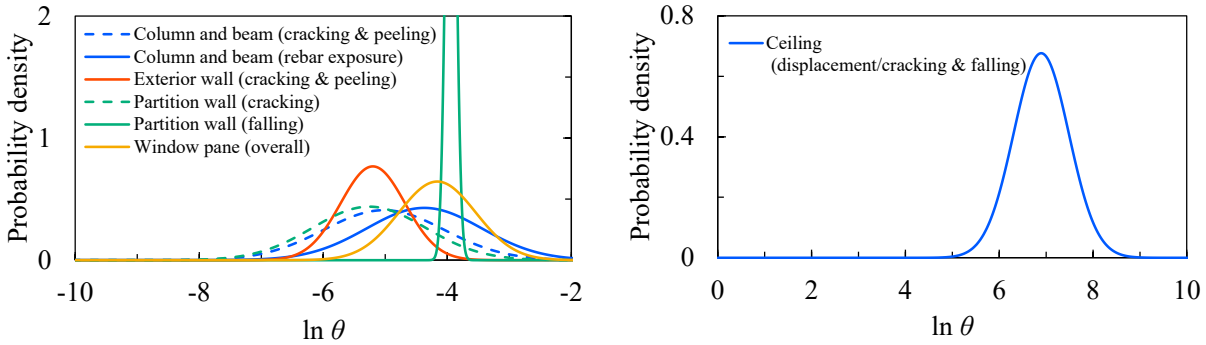
(b) Weakly informative prior distribution: Uniform (a,b).

Fig. 9 Prior distributions of the medians of the fragility curves for Bayesian inference.

Table 3 Parameters for informative prior distributions of the fragility-curve medians for Bayesian inference based on FEMA P-58.

Type of building component	Damage state (ds)	edp_{ij}	Fragility curves (FEMA P-58)			Informative prior distribution	
			DS (number of	θ'_{max}	θ'_{min}	μ	σ

			fragility curves)				
Column and beam	Cracking	PIDA (rad)	DS1 (66)	0.0175	0.0025	-5.02	0.97
	Peeling						
	Rebar exposure		DS2, 3 (114)	0.0322	0.005	-4.37	0.93
Exterior wall	Cracking		DS1 (36)	0.0093	0.0033	-5.20	0.52
	Peeling						
Partition wall	Cracking		DS1, 2 (5)	0.013	0.0021	-5.26	0.91
	Falling		DS3 (3)	0.021	0.018	-3.94	0.08
Window pane	Overall		DS1, DS2 (18)	0.029	0.0084	-4.16	0.62
Ceiling	Displacement Cracking	PFA (cm/s^2)	DS1, DS2, DS3(12)	1783.6	548.8	6.90	0.59
	Falling						



(a) Deformation-sensitive component (b) Acceleration-sensitive component

Fig. 10 Informative prior distributions of the fragility-curve medians for Bayesian inference based on FEMA P-58.

3. Results and discussion

3.1 Effect of prior distributions on the estimated medians of the fragility curves

The influence of differences in the prior distributions used for Bayesian inference on the estimated medians of the fragility curves was analyzed, focusing on four distinct damage states: (1) cracking in partition walls, (2) falling partition walls, (3) displacement/cracking in ceilings, and (4) falling ceilings. Fig. 11 shows comparisons of the fragility curves developed using Bayesian inference using informative and weakly informative prior distributions for each damage state of the building components. The figure also includes fragility curves from FEMA P-58 (FEMA 2018a, b, c), which were used to establish informative prior distributions, alongside the questionnaire survey dataset showing the relationship between damage occurrence (presence/absence) and the estimated structural response quantities. To illustrate estimation uncertainty, the 50% credible interval (25th–75th percentile) of the posterior distribution is also shown in Fig. 11. The

damage ratios for cracking in partition walls and displacement/cracking in ceilings were approximately 30–40%, yielding data for both damaged and undamaged cases. The lognormal distributions set as informative prior distributions for these damage states have a broad shape, leading to no significant differences between the two types of prior distributions. However, the estimated medians of the fragility curves for falling partition walls and ceilings varied depending on the prior distribution type. For falling partition walls, the estimated median of the fragility curve was 0.011 rad with a weakly informative prior and 0.018 rad with an informative prior. For falling ceilings, the estimated median was 1,496 cm/s² with a weakly informative prior and 1,402 cm/s² with an informative prior, indicating only a slight difference. For falling partition walls and ceilings, the damage ratios were less than 20%, resulting in few damaged observations and making the results sensitive to the choice of prior distribution. In the case of falling partition walls, as shown in Fig. 10a, the prior distribution had a sharp shape with a small standard deviation, which was strongly reflected in both the 50th percentile and the 50% credible interval of the posterior distribution. Therefore, when the damage ratio was 30% or higher and the number of data points for both damaged and undamaged cases was sufficient, the difference in the estimation results due to the type of prior distribution was small. This tendency suggests that the estimated medians of the fragility curves primarily reflected the survey dataset. Conversely, when the damage ratio was 20% or less and the number of data points for either damaged or undamaged cases was low, the influence of the informative prior distribution became apparent, indicating that the estimated medians of the fragility curves reflected both the survey dataset and prior information.

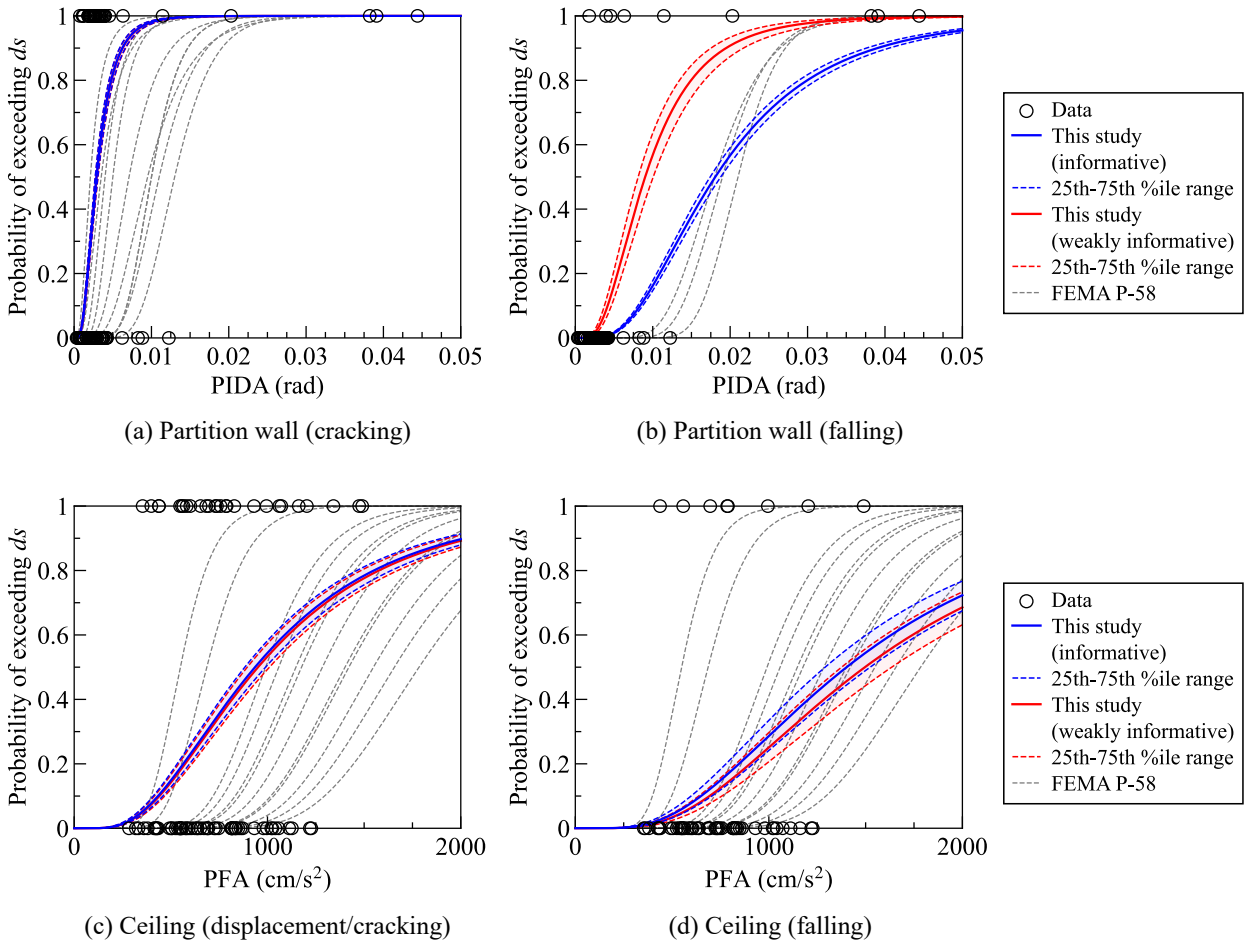


Fig. 11 Comparison of fragility curves developed via Bayesian inference using different prior distributions.

3.2 Developed seismic fragility curves of building components

The medians of the fragility curves were estimated for the damage states of each of the 13 types of building components selected in Section 2.1, using the prior distributions set in Section 2.4. Figs. 12 and 13 show the fragility curves for the deformation-sensitive and acceleration-sensitive components, representing the probability of exceeding a given damage state. To illustrate uncertainties in the estimation results, along with the obtained curve (the 50th percentile), Table 4 presents the 95% credible interval (2.5th–97.5th percentiles) of the posterior distribution, while the figures show the 50% credible interval (25th–75th percentiles). In these figures, to confirm the correspondence between the fragility curves and the questionnaire survey dataset, data were binned into intervals (PIDA: 0.0025 rad; PFA and PGA: 250 cm/s²), and the proportion of damaged cases within each bin (bin damage rate) is shown for bins containing three or more data points. An informative prior distribution was set for columns and beams, exterior walls, partition walls, window panes, and ceilings. For each damage state of each building component, Table 4 presents the edp and the median θ of the fragility curve. The $\hat{R}$ values for all θ in Table 4 are below 1.1, confirming that the estimated posterior

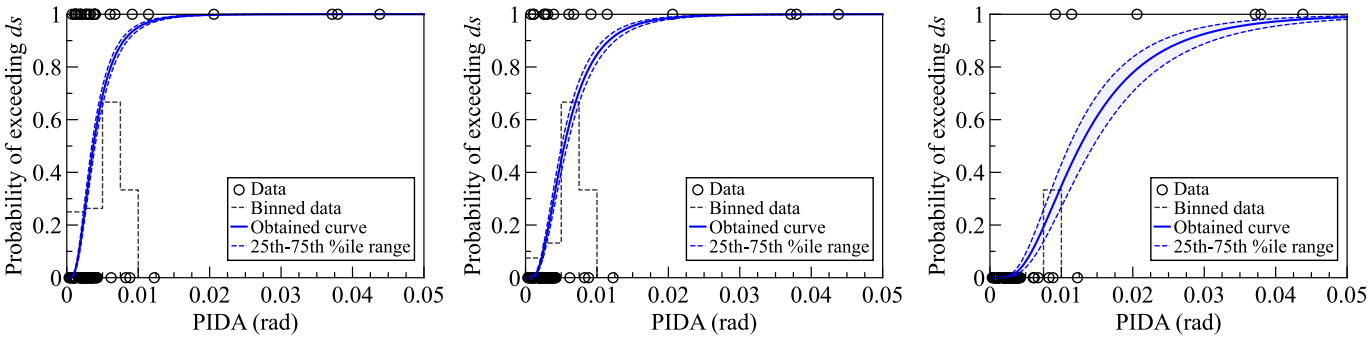
distributions have converged.

First, the estimation results were examined with respect to the damage ratio (Fig. 4) and the type of prior distribution. For cracking in columns and beams, cracking in exterior walls, peeling of exterior walls, cracking to partition walls, and emergency stops of elevators for safety inspections, damage ratios ranged from approximately 30% to 55%. The developed fragility curves reflected the data and generally aligned with the bin damage rates. For emergency stops of elevators for safety inspections, although a weakly informative prior distribution was used, the estimated fragility curves corresponded well with the bin damage rates. Based on the 50% credible intervals, uncertainties in the posterior distributions were small for building components using data from stories, while they were somewhat larger for elevator safety inspections using data from buildings. This confirms that accurately estimating the median of the fragility curve requires a sufficient proportion of damage and adequate data. Next, the damage states of each building component with a damage ratio of 20% or less were analyzed. For rebar exposure in columns and beams, falling partition walls, damage to window panes, and falling ceilings, an informative prior distribution was used; however, the number of bins with calculable bin damage rates was small, resulting in poor correspondence between the developed fragility curves and the bin damage rates. The results estimated using a weakly informative prior distribution corresponded well with the bin damage rates for displacement/cracking in lighting fixtures, and damage to sinks and toilets. However, the correspondence between the developed fragility curves and the bin damage rates for interior door damage, fire door damage, air conditioner damage, and sprinkler head damage was less satisfactory. Although the 50% credible intervals were slightly wider than those for building components with higher damage rates, they did not deviate significantly from the 50th percentile value and were considered acceptable.

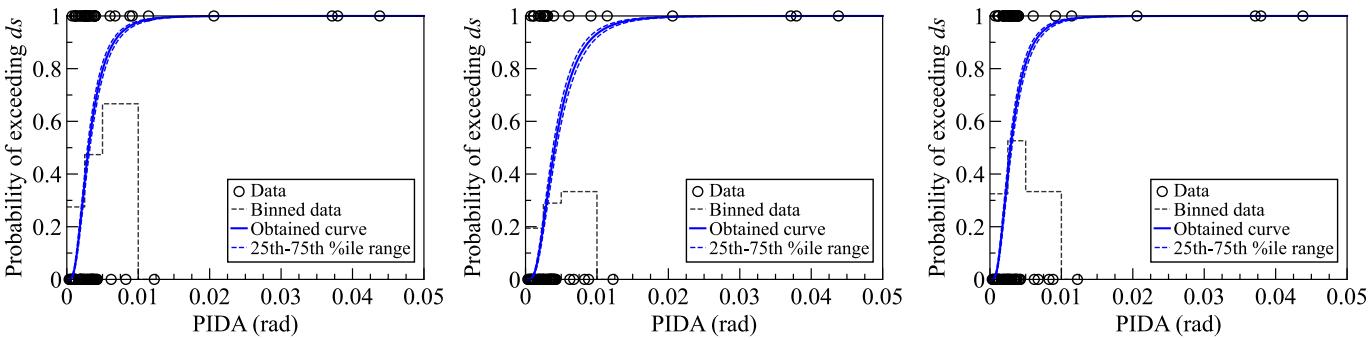
Furthermore, based on the 50th percentile fragility curves, the relationships between different damage states of the same building component and between different building components are discussed. Fig. 14a compares fragility curves for various damage states of columns and beams, exterior walls, and partition walls. The median values for columns and beams increased in the order of cracking, peeling, and rebar exposure, indicating accurate estimates of fragility curves for each damage state. Similarly, for exterior walls, the median values were larger in the order of cracking and peeling. For partition walls, they were larger in the order of cracking and falling, indicating consistency between damage states and the order of fragility curves. As presented in Fig. 10a, although the same informative prior distribution was used for cracking and peeling of columns and beams and of exterior walls, differences in data distributions allowed for the

representation of distinct damage states. Fig. 14b compares fragility curves for ceilings and ceiling-mounted equipment. The fragility curves for displacement/cracking in lighting fixtures, damage to air conditioners, and damage to fire sprinkler heads are comparable to those for falling ceilings. These curves diverge from those for displacement/cracking in ceilings, indicating that ceiling-mounted equipment suffering damage during major incidents, such as falling ceilings, aligns with expectations. Therefore, the developed fragility curves, aligned with actual earthquake damage trends regarding differences in damage levels for the same building components, sequence of damage occurrences, and causal relationships, are effective for evaluating building damage during earthquakes. For example, for a building with a PIDA of 1/200 rad, the probability of rebar exposure in columns and beams is 6%, the probability of cracking in exterior walls and partition walls is 80%, and the probability of water leakage from plumbing is approximately 40%. Therefore, severe structural damage is unlikely, but the building may require repairs to nonstructural components and plumbing.

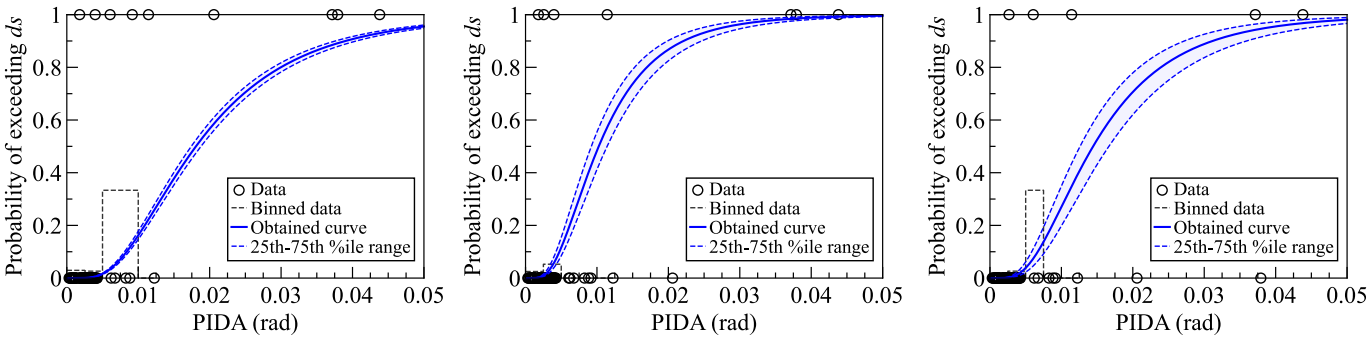
This study identified several issues; further accumulation of damage data is necessary to enhance the estimation accuracy of damage states for such building components. Among the developed fragility curves, those with poor correspondence between bin damage rates and damage data, such as those for damage to interior doors, fire doors, air conditioners, and fire sprinkler heads, present challenges regarding the reliability of the estimation results owing to the limited amount of damage data and the use of weakly informative prior distributions.



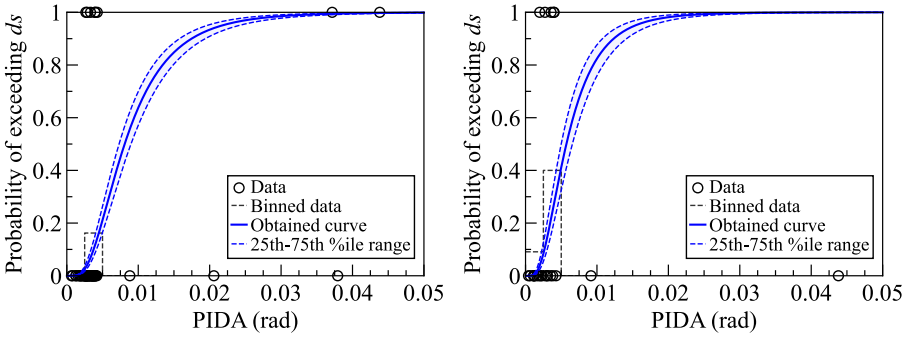
(a) Column and beam (cracking) (b) Column and beam (peeling) (c) Column and beam (rebar exposure)



(d) Exterior wall (cracking) (e) Exterior wall (peeling) (f) Partition wall (cracking)

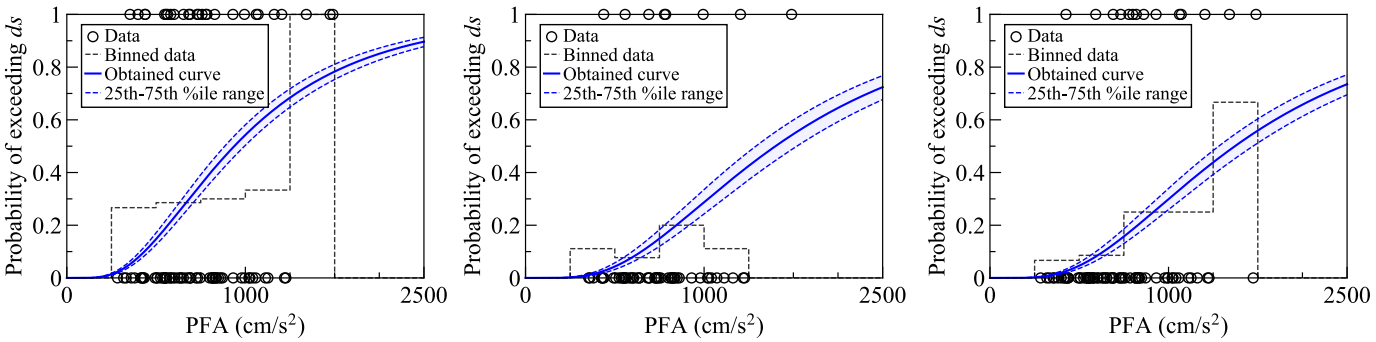


(g) Partition wall (falling) (h) Window pane (i) Interior door



(k) Fire door (l) Plumbing (water leakage)

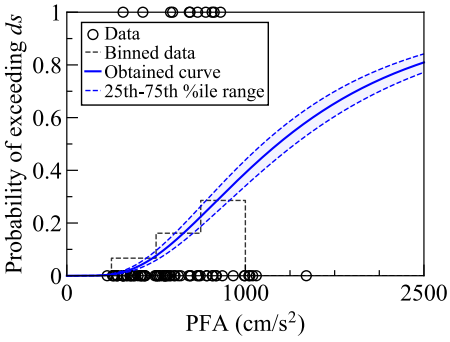
Fig. 12 Developed fragility curves for the deformation-sensitive components, representing the probability of exceeding a given damage state.



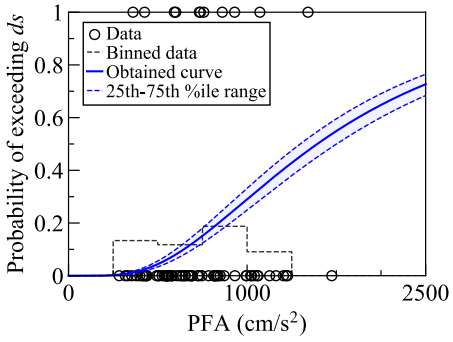
(a) Ceiling (displacement/cracking)

(b) Ceiling (falling)

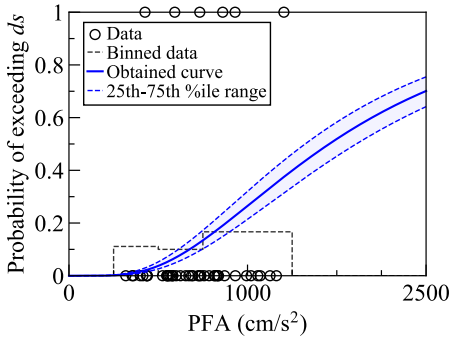
(c) Lighting fixture (displacement/cracking)



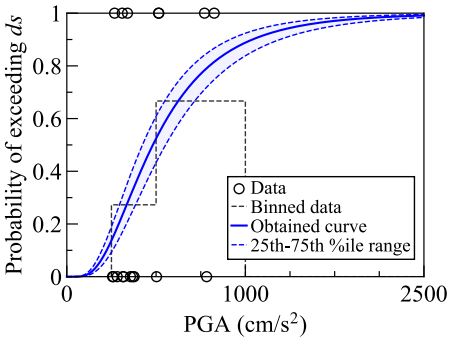
(d) Sink and toilet



(e) Air conditioner



(f) Fire sprinkler head



(g) Emergency stops for safety inspection of elevator

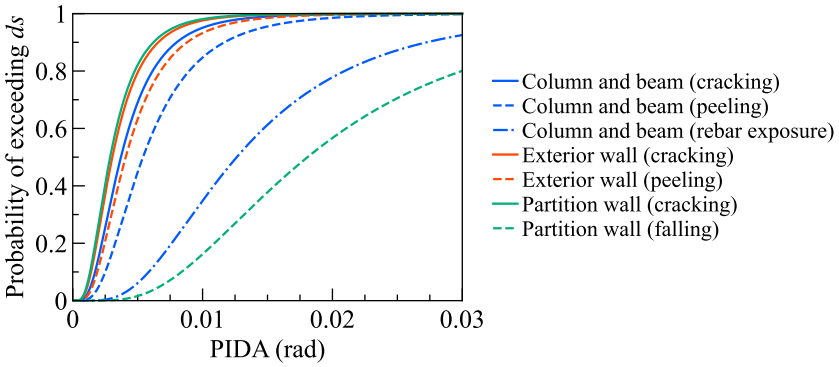
Fig. 13 Developed fragility curves for the acceleration-sensitive components, representing the probability of exceeding a given damage state.

Table 4 Estimated median values of fragility curves for each damage state *ds* of building components (the logarithmic standard deviation $\beta = 0.6$).

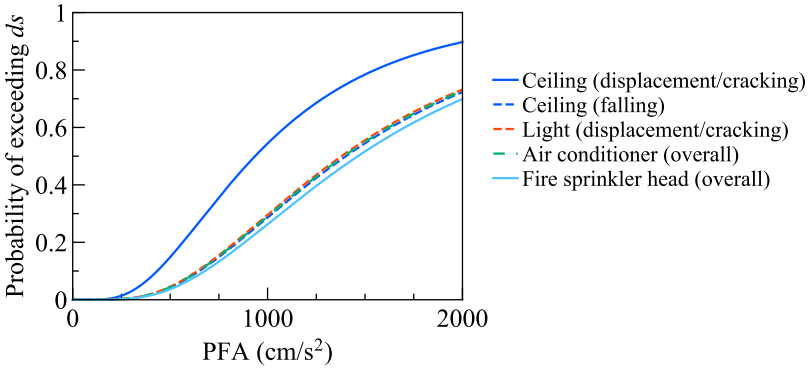
No.	Type of building component	ds	edp	$p(\theta)$	θ	
					50th percentile	2.5th–97.5th percentile
1	Column and beam	Cracking	PIDA (rad)	Informative prior	0.0037	0.0031–0.0044
2		Peeling			0.0054	0.0044–0.0067

3		Rebar exposure		distribution	0.0126	0.0088–0.0192
4	Exterior wall	Cracking			0.0031	0.0026–0.0036
5		Peeling			0.0041	0.0034–0.0049
6	Partition wall	Cracking			0.0029	0.0024–0.0034
7		Falling			0.0181	0.0162–0.0202
8	Window pane	Overall			0.0103	0.0076–0.0142
9	Ceiling	Displacement/cracking	PFA (cm/s^2) *		935.5	790.6–1108.8
10		Falling			1401.8	1110.2–1796.3
11	Interior door	Overall	PIDA (rad)	Weakly informative prior distribution	0.0144	0.0098–0.0223
12	Lighting fixture	Displacement/cracking	PFA (cm/s^2) *		1379.3	1129.7–1706.2
13	Sink and toilet	Overall	PFA (cm/s^2)		1183.5	956.0–1502.2
14	Air conditioner	Overall	PFA (cm/s^2) *		1392.1	1122.3–1736.9
15	Fire door	Overall	PIDA (rad)		0.0081	0.0061–0.0111
16	Fire sprinkler head	Overall	PFA (cm/s^2) *		1463.3	1101.8–1991.4
17	Plumbing	Water leakage	PIDA (rad) **		0.0057	0.0039–0.0086
18	Elevator	Emergency stop for safety inspection	PGA (cm/s^2)		481.8	331.4–707.6

* PFA at one floor above the installation floor, ** Maximum PIDA value across all floors.



(a) Structural and nonstructural components in various damage states.



(b) Ceiling and ceiling-mounted equipment.

Fig. 14 Comparison of fragility curves for each component and equipment.

4. Conclusions

This study applied Bayesian inference to develop fragility curves for structural and nonstructural components and equipment as a function of structural response quantities, using building damage data from questionnaire surveys following the 2016 Kumamoto and 2022 Fukushima-ken Oki earthquakes. Fragility curves were developed based on actual damage data for building components caused by earthquakes, considering only buildings near seismic stations identified through the questionnaire surveys. Observed ground motions were applied to MDOF shear building models constructed from basic building characteristics, and the estimated structural response quantities were correlated with the observed damage states. Bayesian inference was performed using the obtained actual damage data and prior distributions based on fragility curves in FEMA P-58. Through this approach, practically useful fragility curves were developed that integrate empirical data from actual damage with experimental data, even when sample sizes were small.

The developed fragility curves correspond to the following damage states: (1) cracking in columns and beams, (2) peeling of columns and beams, (3) rebar exposure in columns and beams, (4) cracking in exterior walls, (5) peeling of

exterior walls, (6) cracking in partition walls, (7) falling of partition walls, (8) damage to window panes, (9) damage to interior doors, (10) displacement/cracking in ceilings, (11) falling ceilings, (12) displacement/cracking in lighting fixtures, (13) damage to sinks and toilets, (14) damage to air conditioners, (15) damage to fire doors, (16) damage to fire sprinkler heads, (17) water leakage from plumbing, and (18) emergency stops of elevators for safety inspections. Among the developed fragility curves, those for cracking in columns and beams, cracking in exterior walls, peeling of exterior walls, cracking in partition walls, and emergency stops of elevators for safety inspections demonstrate less bias in both damaged and undamaged data, indicating relatively high estimation accuracy. In contrast, fragility curves for damage to interior doors, fire doors, air conditioners, and fire sprinkler heads were developed using weakly informative prior distributions due to the limited amount of damage data, raising reliability concerns. The fragility curves developed for each damage state of the building components were consistent with actual earthquake damage. This consistency includes variations in damage levels within the same component (e.g., partition wall cracking versus falling) and the sequence of damage occurrence (e.g., falling ceilings followed by damage to ceiling-mounted equipment).

The proposed method enabled the construction of 18 fragility curves that reflected earthquake damage observed in actual Japanese buildings. These curves can serve as tools for achieving more reasonable seismic damage assessments of building components for possible future earthquakes in Japan. The characteristics of the fragility curves developed in this study and precautions for their application are summarized as follows:

- Although the data used to develop the fragility curves are limited to the 2016 Kumamoto and 2022 Fukushima-ken Oki earthquakes, the impact of the ground motion characteristics, such as dominant period and duration, is considered minimal because nonlinear seismic response analyses were performed for each building. However, because of the limited survey results from the 2016 Kumamoto Earthquake and the fact that most peak interstory drift angles used as the estimated structural response quantities are based on data below 1/100 rad, the estimation accuracy of the fragility curves may decrease for estimated structural response quantities exceeding 1/100 rad.
- Because most data originate from local government offices, the fragility curves are not intended for use with members or equipment in buildings with specialized functions, such as production plants or power stations.
- Fragility curves evaluate the probability of damage occurring at one or more locations within a specific story of a building. They do not evaluate the number, scale, or specific locations of the damage.
- The applicability of the fragility curves to columns, beams, and exterior walls is limited to RC and SRC structures.

However, the fragility curves for other nonstructural components and equipment are not restricted by structural type.

Future challenges include developing fragility curves for damage to power receiving and transforming equipment, emergency generators, water reservoir tanks, rooftop water tanks, water supply pumps, boilers, plumbing (deformation/cracking), elevators (damage to transport equipment), electrical wiring (displacement/cracking, falling), lighting fixtures (falling), bathtubs, condenser units, and fire detectors. Additionally, the fragility curves for interior doors, fire doors, air conditioners, and fire sprinkler heads rely on weakly informative prior distributions due to the limited amount of damage data, necessitating further data collection and updates to the fragility curves. A common challenge for all building components is the lack of data covering a wide range of estimated structural response quantities.

The proposed method can be generalized to other earthquakes and regions, thereby addressing the limitations and challenges of fragility curves through continuous data collection across multiple earthquake events.

References

Achour N, Miyajima M (2020) Post-earthquake hospital functionality evaluation: The case of Kumamoto Earthquake 2016. Earthq Spectra 36(4):1670–1694. https://doi.org/10.1177/8755293020926180

Aoyama H (1981) Outline of earthquake provisions in the recently revised Japanese building code. Bull N Z Soc Earthq Eng 14(2):63–80. https://doi.org/10.5459/bnzsee.14.2.63-80

Casagrande L, Bonati A, Occhiuzzi A, Caterino N, Auricchio F (2019) Numerical investigation on the seismic dissipation of glazed curtain wall equipped on high-rise buildings. Eng Struct 179:225–245. https://doi.org/10.1016/j.engstruct.2018.10.086

Cremen G, Baker JW (2019) Improving FEMA P-58 non-structural component fragility functions and loss predictions. Bull Earthquake Eng 17(4):1941–1960. https://doi.org/10.1007/s10518-018-00535-7

Donà M, Carpanese P, Follador V, Sbrogiò L, da Porto F (2021) Mechanics-based fragility curves for Italian residential URM buildings. Bull Earthquake Eng 19(8):3099–3127. https://doi.org/10.1007/s10518-020-00928-7

Eidinger J (2009) Fragility of non-structural components, FEMA P-58/BD-3.9.12. Federal Emergency Management

Agency, Washington.

Federal Emergency Management Agency (FEMA) (2018a) Seismic performance assessment of buildings, vol 1 - Methodology, FEMA P-58-1. Available at https://femap58.atcouncil.org/reports (accessed on February 25, 2026).

Federal Emergency Management Agency (FEMA) (2018b) Seismic performance assessment of buildings. In: Implementation guide, vol 2, FEMA P-58-2. Available at https://femap58.atcouncil.org/reports (accessed on February 25, 2026).

Federal Emergency Management Agency (FEMA) (2018c) Seismic performance assessment of buildings. In: Supporting electronic materials and background documentation, vol 3, FEMA P-58-3. Available at https://femap58.atcouncil.org/reports (accessed on February 25, 2026).

Filiatrault A, Sullivan T (2014) Performance-based seismic design of nonstructural building components: The next frontier of earthquake engineering. Earthq Eng Eng Vib 13(S1):17–46. https://doi.org/10.1007/s11803-014-0238-9

Fujii K (2019) Pushover-based seismic capacity evaluation of Uto city hall damaged by the 2016 Kumamoto earthquake. Buildings 9(6):140. https://doi.org/10.3390/buildings9060140

Gautam D, Adhikari R, Rupakhety R (2021) Seismic fragility of structural and non-structural elements of Nepali RC buildings. Eng Struct 232:111879. https://doi.org/10.1016/j.engstruct.2021.111879

Gelman A, Rubin DB (1992) Inference from iterative simulation using multiple sequences. Stat Sci 7(4):457–472. https://doi.org/10.1214/ss/1177011136

Günay S, Mosalam KM (2013) PEER performance-based earthquake engineering methodology, revisited. J Earthquake Eng 17(6):829–858. https://doi.org/10.1080/13632469.2013.787377

Heresi P, Miranda E (2023) RPBEE: Performance-based earthquake engineering on a regional scale. Earthquake Spectra 39(3):1328–1351. https://doi.org/10.1177/87552930231179491

Ioannou I, Bertelli S, Chandler RE, Ohno S, Shibayama A, Suppasri A, Rossetto T (2025) The 2011 Great East Japan earthquake: Fragility of Japanese buildings to ground shaking. Bull Earthquake Eng 23(8):3173–3201. https://doi.org/10.1007/s10518-025-02174-1

Japan Meteorological Agency (2009) Tables explaining the JMA seismic intensity scale, Japan Meteorological Agency. Available at https://www.jma.go.jp/jma/en/Activities/inttable.html (accessed on February 25, 2026).

Moosapoor M, Bessason B, Hrafnkelsson B, Rupakhety R, Bjarnason JÖ, Erlingsson S (2025) Damage-informed

seismic fragility of non-structural elements in South Iceland: A Bayesian hierarchical approach. Eng Struct 338:120504. https://doi.org/10.1016/j.engstruct.2025.120504

Morita K, Kashima T (2017) Study on characteristics of damping ratio of RC/SRC high-rise buildings based on strong motion data. AIJ J Technol Des 23(53):49–52 (in Japanese). https://doi.org/10.3130/aijt.23.49

Mukai T, Watanabe H, Sakashita M, Kashima T, Shiohara H, Kinugasa H, Tani M, Maida Y, Sakuta J, Kaneko O, Tanumea T, Narita N (2021) Investigation for post-earthquake functional use for damaged R/C buildings due to the 2016 Kumamoto earthquake, Building Research Data, No. 204. Building Research Institute National Research and Development Agency, Japan. Available at https://www.kenken.go.jp/japanese/contents/publications/data/204/index.html (accessed on February 25, 2026).

Nagato K, Kawase H (2004) Damage evaluation models of reinforced concrete buildings based on the damage statistics and simulated strong motions during the 1995 Hyogo-ken Nanbu earthquake. Earthq Engng Struct Dyn 33(6):755–774. https://doi.org/10.1002/eqe.376

Nakamura N, Kinoshita T, Ishikawa Y, Ota H, Ikeda S, Ito M, Saito T, Fukuyama H (2013) Response analysis of SRC high-rise building during the 2011 off the pacific coast of Tohoku earthquake. AIJ J Technol Des 19(41):53–58 (in Japanese). https://doi.org/10.3130/aijt.19.53

National Institute of Advanced Industrial Science and Technology (AIST) (2013) QuiQuake: Quick estimation system for earthquake map triggered by observed records. Available at https://gbank.gsj.jp/QuiQuake/index.en.html (accessed on February 6, 2023).

National Research Institute for Earth Science and Disaster Resilience (NIED) (2019a) NIED F-net. National Research Institute for Earth Science and Disaster Resilience. https://doi.org/10.17598/nied.0005

National Research Institute for Earth Science and Disaster Resilience (NIED) (2019b) 7.5-Arc-Second Japan Engineering Geomorphologic Classification Map. National Research Institute for Earth Science and Disaster Resilience. https://doi.org/10.17598/nied.0011

National Research Institute for Earth Science and Disaster Resilience (NIED) (2019c) NIED K-NET, KiK-Net. National Research Institute for Earth Science and Disaster Resilience. https://doi.org/10.17598/nied.0004

Neal RM (2011) MCMC using Hamiltonian dynamics. In: Brooks S, Gelman A, Jones G, Meng XL (eds), Handbook of Markov chain Monte Carlo. Chapman & Hall/CRC, p 113–162. https://doi.org/10.1201/b10905-6

Nishino T (2024) Post-earthquake building services downtime distribution: A case study of the 2016 Kumamoto, Japan, earthquake. Archit Struct Constr 4(2–4):227–240. https://doi.org/10.1007/s44150-024-00113-3

Nishino T, Hada A, Kawase H, Matsushima S (2025) Empirical seismic fragility function for fire doors based on inspection data from the 1995 Kobe earthquake and its use in post-earthquake fire risk assessments. J Build Eng 104:112362. https://doi.org/10.1016/j.jobe.2025.112362

Nishino T, Morii T, Okazawa R, Notake H, Hada A, Matsui T (2026) Empirical model of post-earthquake restoration time for building components based on data from the 2022 Fukushima-ken Oki earthquake in Japan. Earthq Engng Struct Dyn. https://doi.org/10.1002/eqe.70229

Okazawa R, Sugino M, Hayashi Y (2018) Modeling of super high-rise buildings and response properties against Ricker wavelet—Damage prediction for super high-rise buildings in Osaka against pulse-like ground motions: Part 1. J Struct Constr Eng 83(745):421–430 (in Japanese). https://doi.org/10.3130/aijs.83.421

Perrone D, Calvi PM, Nascimbene R, Fischer EC, Magliulo G (2019) Seismic performance of non-structural elements during the 2016 Central Italy earthquake. Bull Earthquake Eng 17(10):5655–5677. https://doi.org/10.1007/s10518-018-0361-5

Porter K, Kennedy R, Bachman R (2007) Creating fragility functions for Performance-Based Earthquake Engineering. Earthquake Spectra 23(2):471–489. https://doi.org/10.1193/1.2720892

Rossi L, Stupazzini M, Parisi D, Holtschoppen B, Ruggieri G, Butenweg C (2020) Empirical fragility functions and loss curves for Italian business facilities based on the 2012 Emilia-Romagna earthquake official database. Bull Earthquake Eng 18(4):1693–1721. https://doi.org/10.1007/s10518-019-00759-1

Stan Development Team (2026) Stan user's guide, version 2.38.0. https://mc-stan.org

Suwa H, Kanda J (2008) Damage ratio curves of building equipments by using the damage database due to 1995 Hyogoken Nanbu earthquake. J Struct Constr Eng (Trans AIJ) 73(633):1935–1941, (in Japanese). https://doi.org/10.3130/aijs.73.1935

Taghavi S, Miranda E (2003) Response assessment of nonstructural building elements, PEER Report 2003–05. Pacific Earthquake Engineering Research Center, University of California Berkeley. Available at https://peer.berkeley.edu/sites/default/files/0305_s._taghavi_e._miranda_.pdf (accessed on March 2, 2026).

Takeda T, Sozen MA, Nielsen NN (1970) Reinforced concrete response to simulated earthquakes. J Struct Div

96(12):2557–2573. https://doi.org/10.1061/JSDEAG.0002765

Umemura H, Watabe M, Ishiyama Y, Fukuta T (1984) Follow-up of new earthquake resistant regulations for buildings in Japan. In: Proceedings of the 8th world conference on earthquake engineering, p 739–746

Wang Z, Zentner I, Zio E (2018) A Bayesian framework for estimating fragility curves based on seismic damage data and numerical simulations by adaptive neural networks. Nucl Eng Des 338:232–246. https://doi.org/10.1016/j.nucengdes.2018.08.016

Zuccaro G, Perelli FL, De Gregorio D, Cacace F (2021) Empirical vulnerability curves for Italian mansory buildings: Evolution of vulnerability model from the DPM to curves as a function of accelertion. Bull Earthquake Eng 19(8):3077–3097. https://doi.org/10.1007/s10518-020-00954-5

Statements and Declarations

Funding The authors declare that no funds, grants, or other support were received during the preparation of this manuscript.

Competing Interests The authors have no relevant financial or non-financial interests to disclose.

Author Contributions Takahiro Matsui: Methodology, Formal analysis, Investigation, Writing – original draft, Visualization. Takeshi Morii: Conceptualization, Methodology, Formal analysis, Investigation, Writing – original draft. Rie Okazawa: Methodology, Formal analysis, Investigation, Writing – original draft. Tomoaki Nishino: Conceptualization, Methodology, Investigation, Writing – original draft. Hiroaki Notake: Methodology, Investigation, Writing – review & editing. Aya Hada: Investigation, Writing – review & editing.

Data Availability The raw data collected from the questionnaire survey are not publicly available because the respondents did not provide consent for data sharing. The derived data supporting the findings of this study are available from the corresponding author upon reasonable request.